applied sciences

MDPI

Article

Experimental Analysis of Heat and Flow Characteristics on Inclined and Multiple Impingement Jet Heat Transfer Using Optimized Heat Sink

Altug Karabey [1,*] and Dogan Yorulmaz [2]

[1] Department of Mechanical Engineering, Faculty of Engineering, Van Yuzuncu Yil University, Van 65080, Turkey
[2] Department of Mechanical Engineering, Institute of Naturel and Applied Science, Van Yuzuncu Yil University, Van 65080, Turkey; dogann.yorulmaz@gmail.com
* Correspondence: akarabey@yyu.edu.tr; Tel.: +90-5334881658

Abstract: Thermal management at a high heat flux is crucial for electronic devices, and jet impingement cooling is a promising solution. The heat transfer properties of a rectangular-finned heat sink are investigated under angled and multi-impingement jet configurations in this study. Experiments were conducted with three different nozzle diameters, three different heat sink angles, three dimensionless nozzle-to-heat sink distance ratios, and five different velocity values. As a result, the obtained data are presented as Nu-Re graphs, and the impacts of the parameters on heat transfer (HT) are analyzed. It is concluded that the Nusselt number increases with the increasing nozzle diameter and Reynolds number, whereas it decreases with increasing distance between the nozzle and the heat sink. When comparing the angle values under an identical flow velocity, nozzle diameter, and dimensionless h/d distance experimental conditions, it was found that the Nusselt numbers were very close to each other. Under constant heat flux and for all investigated angles, the highest Nusselt number for the rectangular-finned inclined heat sink was observed at a 10° heat sink inclination, a nozzle diameter of D = 40 mm, a dimensionless distance of h/d = 6, and a flow velocity of 9 m/s. This study deepens the understanding of the heat transfer mechanism of impinging jets and provides an efficient method framework for practical applications.

Keywords: forced convection; heat transfer enhancement; multi-nozzle impingement jet

check for updates

Academic Editors: Feng Zhang and Yong Li

Received: 7 January 2025
Revised: 20 February 2025
Accepted: 24 February 2025
Published: 1 March 2025

Citation: Karabey, A.; Yorulmaz, D. Experimental Analysis of Heat and Flow Characteristics on Inclined and Multiple Impingement Jet Heat Transfer Using Optimized Heat Sink. *Appl. Sci.* **2025**, *15*, 2657. https://doi.org/10.3390/app15052657

Copyright: © 2025 by the authors. Licensee MDPI, Basel, Switzerland. This article is an open access article distributed under the terms and conditions of the Creative Commons Attribution (CC BY) license (https://creativecommons.org/licenses/by/4.0/).

1. Introduction

The increasing energy costs today have made achieving energy efficiency a necessity. Consequently, the increasing significance of HT in both daily life and industrial practices highlights the need for studies aiming to improve HT mechanisms. Furthermore, with technological advancements, the cooling of microprocessors, electromechanical systems, and circuit components producing high heat flux has become increasingly significant. The elevated junction temperatures of these systems under high heat flux reduce the performance and lifespan of the devices in which they are used. To maintain the temperatures of systems with high heat flux at optimal levels, various cooling methods are employed. These include air impingement jet cooling [1–3], liquid jet cooling [4], microchannel cooling [5], micropump cooling [6], and spray cooling [7–10]. In the context of impinging jet applications, studies examining heat transfer characteristics are as important as those examining flow characteristics. In fluid dynamics, research conducted on fluid–structure

interaction systems using various approaches offers unique benefits in determining flow characteristics [11,12].

Previous studies reported that impinging jets are a fast, economical, and efficient method for mass and HT over target surface areas [13].

Air impingement jet processes represent the upper limit of forced convection achieved through airflow considering the localized HT. Consequently, applications of cooling electronic components with air impingement jets have gained considerable importance. The operating temperatures of electronic systems are critical factors influencing their performance. Thermal stress caused by operating temperatures leads to system malfunctions and significant efficiency losses. Cooling heated components with either a single impingement jet or arrays of impingement jets is a key application for protecting such electronic circuits [14].

The HT and flow characteristics of multi-impingement jets depend on various parameters, such as the velocity profile at the jet outlet, jet geometry, the distance between the jet and the heat sink, the temperature difference between the jet and the heat sink, and the flow characteristics within the jet [15]. The superior HT capability of multi-impingement jets is primarily attributed to the absence of a boundary layer in the stagnation region and the distribution of cooling air across the impinged plate [16].

Many experimental and numerical studies have examined variations in one or more of these parameters in HT with multi-impingement jets. Previous studies analyzed various heat exchanger types (e.g., square, solid/hollow cylindrical, angled cross-sections) and jet outlet geometries and proposed many designs and recommendations. However, applications, analyses, and comparisons of multi-angled impingement jet setups remain relatively scarce.

Bhaumik et al. [17] developed a numerical model to analyze perforated finned heat sinks in staggered and inline arrangements, and they reported that staggered fin configurations exhibited more uniform thermal distribution. They also highlighted that the circular perforations on the fins contributed to material savings, increased thermal efficiency, and overall HT effectiveness.

Kim et al. [18] experimentally investigated the impact of fin usage and the distance between jet nozzles on HT during the cooling of a heated heat sink with a series of inline jets. Their study, which was carried out at an RE of 15,000, revealed that while fin usage relatively homogenized HT, it did not lead to significant increases in average values.

Yang et al. [19] examined the effects of varying immersion heights of jet nozzles arranged in a 16 $\times$ 5 array within a channel on HT and flow motion for different REs (10,000–30,000) using both experimental and numerical methods. They determined that gradually increasing the nozzle length towards the channel outlet improved and homogenized HT.

Rabbani and Singh [20] conducted a numerical analysis using a large eddy simulation to investigate the impact of different impingement heights on the local HT of a slot jet-cooled channel at REs of 4000, 8000, and 12000. They concluded that the Nusselt number (Nu) increased with the increase in the Reynolds number (Re) and that, at a constant Re, the Nu increased with decreasing distance between the slot jet and the target plate. However, they noted that variations in Re had a more pronounced effect on the Nu than changes in the jet-to-target distance.

Karabey and Arvasi [21] investigated eleven distinct characteristics over three levels each to determine the ideal conditions for multi-jet impingement applications. The Nu served as the performance measure, and an $L_{27}(3^{11})$ orthogonal array was chosen as the experimental design. Optimal results were obtained when the Nu was computed using the nozzle diameter under the following specified conditions: a pipe diameter of 40 mm, air velocity of 9 m/s, vertical spacing between fins of 20 mm, heat flux of 400 W, fin width of

15 mm, fin angle of 30°, horizontal spacing between slices of 15 mm, heat receiver angle of 10°, horizontal spacing between fins of 20 mm, and a nozzle-to-heat receiver distance ratio (h/d) of eight. A comparison of the finned, optimum heat receiver versus a flat surface under ideal circumstances showed a 28.61% enhancement in heat transmission using the finned heat receiver.

Karabey et al. [22] used computational and experimental techniques to examine the HT and flow characteristics of a heat sink with optimized rectangular fins subjected to a single impingement jet using the Taguchi experimental $L_{18}(2^1 * 3^7)$ design approach. The heat sink, designed for jet impingement cooling, was evaluated at six jet velocities (4, 5, 6, 7, 8, and 9 m/s), four nozzle diameters (D = 40, 50, 63, and 75 mm), and three nozzle-to-target distances (h/d = 1, 2, and 3). Alterations in the mean target surface temperature were assessed, and fluctuations in Nus and Res were calculated. The findings were numerically simulated with ANSYS Fluent 19 software. Experimental and numerical findings were compared using Nu-Re diagrams, demonstrating that the average Nu increased proportionately with Re. The Nu decreased as the distance between the nozzle and the heat receiver grew. The agreement between the experimental and numerical findings was validated.

Guresci et al. [23] conducted a numerical analysis of the HT and flow characteristics of hexagonal finned heat sinks optimized by the Taguchi experimental $L_{18}(2^1 * 3^7)$ design technique for channel flow. The ANSYS Fluent Icepak module was used for computational fluid dynamics research on two optimized heat sinks, including three distinct fin heights and five varying flow velocities. For all fin heights, the Nusselt number rose with the Reynolds number for the OH-1 and OH-2 heat sinks. Furthermore, the findings indicated a reduction in the friction factor with an increase in the Reynolds number for all fin heights. CFD data were used to derive changes in Nu-Re and f-Re, which were then compared to the experimental findings. It was concluded that the numerical and experimental findings were congruent.

Jung et al. [24,25] compared the HT characteristics of standard and inclined jet arrays. Their findings indicated that inclined jet designs exhibited superior HT performance compared to standard jet configurations. However, strong crossflow in the downstream jet regions significantly reduced HT.

Heo et al. [26] conducted a theoretical study to evaluate jet inclination angles. Their study, aimed at optimizing the placement of inclined impingement jets, found that an injection hole angle of approximately 60° on a concave surface achieved the highest cooling efficiency.

Ravanji and Zargarabadi [27] investigated the HT effects of various fin geometries—square, circular, rectangular, and elliptical—arranged in a circular pattern under a single impingement jet with identical wetted surface areas. Elliptical fins provided the best cooling performance on roughened surfaces as they created weaker recirculation zones and achieved higher velocities around the fins. Both numerical and experimental results showed that elliptical fins significantly reduced local temperatures in the impingement and wall jet regions. Consequently, the area-averaged Nu improved by 47–54% compared to a flat surface.

Lu et al. [28] investigated the effects of microfin height and geometry (rectangular and pentagonal) on HT in jet impingement cooling. They found that fin height is a critical parameter in enhancing HT, while the pressure drop remained nearly identical to that of a smooth, flat surface.

Smith et al. [29] investigated the combined use of water jets and conical surface modifications for cooling power electronics in automotive applications. Despite only a 1–3% increase in the HT area, they observed a decrease of 3.5–7.5% in the average surface temperature rise. They concluded that conical surface modifications could be effective in achieving

uniform surface temperatures, potentially improving device performance and extending operational lifespan.

Nourin and Amano [30] reported that, in multi-jet impingement cooling, a target surface with hemispherical dimples demonstrated 5–10% greater HT efficiency compared to a smooth surface.

In this study, the effective parameters of the heat transfer of the heat sink, which was previously optimized using the Taguchi optimization method, were investigated according to the single variable method. The effects of varying heat sink angles, nozzle diameter, h/d ratio, and velocity under constant heat flux conditions were analyzed for the optimized heat sink. Considering the importance of analyzing the effect of the heat sink angle, nozzle diameter, dimensionless distance, and flow rate variables on the heat transfer performance of jet impingement systems, this study aims to provide scientifically proven answers to the industry. In the field of cooling applications with impinging jets, it is thought that the analyses made using the geometry of longitudinally and laterally arranged fin pairs, which are rarely encountered in studies, will contribute to the literature and industrial applications. When the parameters affecting impingement jet cooling are examined, the analyses performed according to the single variable method will provide new perspectives for the optimization of jet impingement cooling systems and offer potential improvements in thermal performance and efficiency.

2. Materials and Methods

2.1. Experimental Parameters and Planning

On the basis of this study, controllable parameters were chosen due to the influence they might have on the HT characteristics. All the parameters were chosen to be at 3 levels, and accordingly, the $L_{27}(3^{11})$ orthogonal series shown in Table 1 was chosen as the experimental plan [21].

Table 1. $L_{27}(3^{11})$ experimental plan [21].

EXPERIMENTS											
	A	**B**	**C**	**D**	**E**	**F**	**G**	**H**	**I**	**J**	**K**
1	25 mm	6	5 m/s	10°	15°	2222 W/m^2	15 mm	10 mm	10 mm	10 mm	10 mm
2	25 mm	6	5 m/s	10°	30°	3333 W/m^2	30 mm	15 mm	15 mm	15 mm	15 mm
3	25 mm	6	5 m/s	10°	45°	4444 W/m^2	45 mm	20 mm	20 mm	20 mm	20 mm
4	25 mm	7	7 m/s	20°	15°	2222 W/m^2	15 mm	15 mm	15 mm	15 mm	20 mm
5	25 mm	7	7 m/s	20°	30°	3333 W/m^2	30 mm	20 mm	20 mm	20 mm	10 mm
6	25 mm	7	7 m/s	20°	45°	4444 W/m^2	45 mm	10 mm	10 mm	10 mm	15 mm
7	25 mm	8	9 m/s	30°	15°	2222 W/m^2	15 mm	20 mm	20 mm	20 mm	15 mm
8	25 mm	8	9 m/s	30°	30°	3333 W/m^2	30 mm	10 mm	10 mm	10 mm	20 mm
9	25 mm	8	9 m/s	30°	45°	4444 W/m^2	45 mm	15 mm	15 mm	15 mm	10 mm
10	32 mm	6	7 m/s	30°	15°	3333 W/m^2	45 mm	10 mm	15 mm	20 mm	10 mm
11	32 mm	6	7 m/s	30°	30°	4444 W/m^2	15 mm	15 mm	20 mm	10 mm	15 mm
12	32 mm	6	7 m/s	30°	45°	2222 W/m^2	30 mm	20 mm	10 mm	15 mm	20 mm
13	32 mm	7	9 m/s	10°	15°	3333 W/m^2	45 mm	15 mm	20 mm	10 mm	20 mm
14	32 mm	7	9 m/s	10°	30°	4444 W/m^2	15 mm	20 mm	10 mm	15 mm	10 mm
15	32 mm	7	9 m/s	10°	45°	2222 W/m^2	30 mm	10 mm	15 mm	20 mm	15 mm
16	32 mm	8	5 m/s	20°	15°	3333 W/m^2	45 mm	20 mm	10 mm	15 mm	15 mm
17	32 mm	8	5 m/s	20°	30°	4444 W/m^2	15 mm	10 mm	15 mm	20 mm	20 mm
18	32 mm	8	5 m/s	20°	45°	2222 W/m^2	30 mm	15 mm	20 mm	10 mm	10 mm
19	40 mm	6	9 m/s	20°	15°	4444 W/m^2	30 mm	10 mm	20 mm	15 mm	10 mm
20	40 mm	6	9 m/s	20°	30°	2222 W/m^2	45 mm	15 mm	10 mm	20 mm	15 mm
21	40 mm	6	9 m/s	20°	45°	3333 W/m^2	15 mm	20 mm	15 mm	10 mm	20 mm
22	40 mm	7	5 m/s	30°	15°	4444 W/m^2	30 mm	15 mm	10 mm	20 mm	20 mm
23	40 mm	7	5 m/s	30°	30°	2222 W/m^2	45 mm	20 mm	15 mm	10 mm	10 mm

Table 1. *Cont.*

EXPERIMENTS											
	A	**B**	**C**	**D**	**E**	**F**	**G**	**H**	**I**	**J**	**K**
24	40 mm	7	5 m/s	30°	45°	3333 W/m^2	15 mm	10 mm	20 mm	15 mm	15 mm
25	40 mm	8	7 m/s	10°	15°	4444 W/m^2	30 mm	20 mm	15 mm	10 mm	15 mm
26	40 mm	8	7 m/s	10°	30°	2222 W/m^2	45 mm	10 mm	20 mm	15 mm	20 mm
27	40 mm	8	7 m/s	10°	45°	3333 W/m^2	15 mm	15 mm	10 mm	20 mm	10 mm

Thanks to the Taguchi experimental design, only 27 experiments were conducted using the $L_{27}(3^{11})$ experimental plan rather than conducting 3^{11} = 177,147 experiments using the traditional experimental design methods and complete factorial design. In these experiments, to observe the effects of disruptive and random factors, each experiment was conducted twice at different times, and 54 experiments were conducted in total. "Performance statistic" was shown as the optimization criterion. Performance values of the Nusselt number were calculated to observe the effects of parameters on the optimization criterion.

As seen in Table 2, optimum results were achieved with a 40 mm nozzle diameter, 9 m/s air velocity, 20 mm vertical distance between slices, 4444 W/m^2 heat flux, 20 mm vertical distance between fins, 15 mm fin width, 30° fin angle, 15 mm horizontal distance between slices, 10° heat sink angle, 20 mm horizontal distance between fins, and 8 h/d (the ratio of the nozzle diameter to the nozzle–heat sink distance) [21].

Table 2. Optimization results using the Nusselt numbers [21].

		Parameters											**Performance Value**		
		A	**B**	**C**	**D**	**E**	**F**	**G**	**H**	**I**	**J**	**K**	**Nusselt Number**		
		mm	**h/d**	**m/s**	**α**	**β**	**W**	**mm**	**a**	**c**	**f**	**e**	**Estimation**	**Confidence Range**	**Real**
Nusselt Number	Optimum level	3 •	3 □	3 ♦	1 +	2 ◊	3 ▲	1 ■	3 ✡	3 Δ	2 °	3 *	39.77	37.80–41.74	38.65
	Optimum value	40	8	9	10	30	400	15	20	20	15	20			

•: 1st degree effective ♦: 2nd degree effective *: 3rd degree effective ▲: 4th degree effective Δ: 5th degree effective ■: 6th degree effective ◊: 7th degree effective °: 8th degree effective +: 9th degree effective ✡: 10th degree effective □: 11th degree effective.

In this study, the HT characteristics of a rectangular finned heat sink, previously optimized using the Taguchi $L_{27}(3^{11})$ experimental design method, were investigated under angular and multi-impingement jet conditions. For the optimized heat sink, the effects of varying heat sink angles, nozzle diameters, h/d ratios, and velocity values under constant heat flux conditions were analyzed. Experiments were conducted using three different nozzle diameters (d = 25, 32, and 40 mm) with nine nozzles each, three different h/d ratios (h/d = 6, 7, and 8), and five velocity values (V = 5, 6, 7, 8, and 9 m/s).

Figure 1 presents a schematic representation of the experimental setup. The system is mostly composed of aluminum and reinforced with a steel pipe structure. It consists of an impingement jet system, a data collection thermography system, heat sinks, and a thermally insulated portion fitted with heating components that provide continuous heat flux. Data are sent to a computer for storage and further analysis. The impingement jet system comprises an axial-flow fan unit, a butterfly valve, reducers, and a multi-nozzle configuration, including three distinct nozzle sizes. Air cooling is accomplished using a blower, with a butterfly valve at the fan output regulating air velocity. Air is designated as the operating fluid in the system.

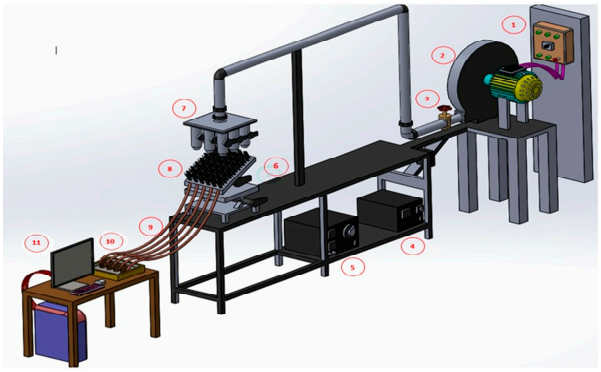

Figure 1. Test setup. (1) Velocity regulator, (2) fan, (3) valve, (4) regulator, (5) variac, (6) mechanism for the lifting jack and heat sink angle, (7) impingement multi-jet nozzles, (8) angularly adjustable finned heat sink, (9) thermocouples, (10) datalogger, and (11) computer.

The experimental configuration for measurements comprises a jack, a flat surface with an adjustable heat sink angle, a heating unit, a base plate, and rectangular finned heat sinks. The dimensionless h/d distances are modified using a jack positioned underneath the heating unit. The heating unit, including square base plates and finned heat sinks, measures 300 mm − 300 mm × 170 mm. It mainly comprises an electric heater, a 50 mm-thick fireproof brick, and thermal insulation. The electric heater, situated on the fireproof brick, has dimensions of 250 mm × 250 mm and functions at 200 W with a voltage of 50 V and a current of 4 A. The electrical power delivered to the heater is regulated by a variac transformer to maintain a consistent heat flux over the test plate. The base plate, composed of aluminum (Al 1050), is 300 mm × 300 mm × 5 mm. The rectangular fins affixed to the base plate measure 2 mm in thickness, 15 mm in width, and 100 mm in height, fabricated from the same aluminum alloy (see Figure 2).

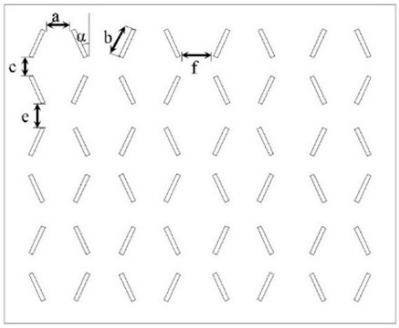

Figure 2. The general characteristics of the heat sink.

A thermal compound was used between the fins and the base plate, as well as underneath the fins, where they interfaced with the base plate to reduce contact resistance to HT. Fifteen thermocouples were positioned on the plate to assess the average surface temperature, two were designated for ambient temperature monitoring, and one was used to evaluate air temperature. Thermocouple measurements were obtained using a data collecting system Ordel UDL100 Data Logger (Ordel Electronic, Ankara, Turkey) and SBA200 signal converter (Ordel Electronic, Ankara, Turkey) linked to a computer, with the average values representing the steady-state surface temperature of the test surface. Copper–constantan thermocouples were calibrated in a thermostat with an accuracy of ±0.1 °C prior to their use in the tests. The system was run for 190 to 200 min to achieve steady-state conditions. Average velocities were measured at the center of the jet nozzle exit using a Testo 400 anemometer (Testo SE & Co. KGaA, Schwarzwald, Germany).

The controllable parameters selected based on their potential impact on HT characteristics and the values used in the experiments are presented in Table 3.

Table 3. Variables analyzed in the experiments.

Variables	Explanation	Value
a	The horizontal distance between fins (mm)	20
b	Fin width (mm)	15
c	The vertical distance between fins (mm)	20
e	The vertical distance between slices (mm)	20
f	The horizontal distance between slices (mm)	15
h_k	Fin height (mm)	100
α	Fin angle (degree)	30°
β	Angle of heat sink (degree)	10°-20°-30°
h/d	Dimensionless distance between the nozzle–heat sink	6-7-8
d	Nozzle diameter (mm)	25-32-40
V	Velocity of fluid (m/s)	5-6-7-8-9

2.2. Data Reduction

The steady-state condition of the HT through the air may be stated as given below [23]:

$$Q_{tot} = Q_{conv} + Q_{rad} + Q_{cond} \quad (1)$$

$$\dot{Q}_{conv} = \dot{m}C_p(T_{out} - T_{in}) = V^2/R = VI \quad (2)$$

The HT from the test unit by convection can be calculated as follows [13]:

$$Q_{conv} = h_{ave}A_s(T_{yave} - T_{jet}) \quad (3)$$

The metal base plate and fins were meticulously cleaned and polished. The operational temperature was maintained within standard parameters. In this context, the radiative heat loss was deemed to be below 5% of the total input to the pin-fin arrays. Consequently, the radiative heat loss from this component may be disregarded. Considering these findings and the effective insulation of the section, together with the thermocouple readings at the outside surface of the heating section, which are almost equivalent to the ambient temperature, the last two elements of Equation (1) may be disregarded.

These assumptions are shortened in Equation (1) given as follows:

$$Q_{total} = Q_{conv} \quad (4)$$

The average HT coefficient was attained from Equations (1)–(3) given as follows:

$$h_{ave} = \frac{Q_{conv}}{A_s(T_{yave} - T_{jet})} \quad (5)$$

Previous studies employed both the projection area and total HT area as metrics for the HT surface area. The whole HT region was used in the current investigation. This region pertains to the overall HT area, including both fins and the base plate, and may be delineated as follows [2,14]:

$$A_s = WL + N[(2bh_k + (2th_k)] \quad (6)$$

where W denotes the width of the base plate, L signifies its length, N represents the number of fins, b indicates the fin breadth, t relates to the thickness of the heat sink, and h_k pertains to the height of the rectangular fins.

Although most jet-impinging applications are turbulent, laminar jets are also encountered in many industrial applications, such as microelectronic devices, miniature geometry, and jets of highly viscous fluid. Most of the published studies on jet impingement cooling consider forced convection a heat transfer mode. In these studies, the Buoyancy effect is neglected. Therefore, the Buoyancy effect is neglected in this study. However, it cannot be neglected for the low Reynolds number laminar flow. For laminar jet flows, the impinging regime may fall into natural, forced, or mixed convection, depending on the relative strengths of the inertia/viscous forces and the buoyancy forces involved [31,32].

The Prandtl number is independent of temperature. In the experiments conducted in this study, the air temperature was approximately 20 °C. Nu served as a performance metric. The inner diameter of the nozzle and the thermal conductivity of the fluid can be used in the calculation of the Nu in Equation (7) as proposed by Karabey and Arvasi [21]:

$$Nu = \frac{hD_h}{k} \tag{7}$$

The velocity recorded at the nozzle center was used to compute the average velocity throughout the nozzle section in a turbulent flow. The mean velocity of the channel can be determined as follows [23,33]:

$$U_{ave} = 0.817U_0 \tag{8}$$

Re is calculated as follows [22]:

$$Re = \frac{\rho U_{ave} D_h}{\mu} \tag{9}$$

where U_{ave} denotes the average velocity at the nozzle section, ρ signifies the fluid density, and μ indicates the dynamic viscosity of the fluid. The thermophysical properties of the fluid at the nozzle exit were ascertained using this parameter. The properties of the fluid used in these analyses are given in Table 4 [33].

Table 4. Properties of fluid.

Properties	Air
Density (kg m^{-3})	1.118
Dynamic viscosity (kg m^{-1} s^{-1})	1.83×10^{-5}
Thermal conductivity (W m^{-1} K^{-1})	0.026
Specific heat capacity, (J kg^{-1} K^{-1})	1007

2.3. Uncertainty Analysis

Uncertainty analysis is a crucial technique used to evaluate the degree to which mistakes from experimental measurements distort the answer from the true outcome. Employing the uncertainty analysis (Equation (10)) established by Kline and McClintock [34], a maximum uncertainty of 4.25% was determined for the Re, while a maximum uncertainty of 9.26% was identified for the Nu.

$$W_R = \left[\left(\frac{\partial R}{\partial x_1} W_1 \right)^2 + \left(\frac{\partial R}{\partial x_2} W_2 \right)^2 + \cdots + \left(\frac{\partial R}{\partial x_n} W_n \right)^2 \right]^{\frac{1}{2}} \tag{10}$$

The individual contributions to the uncertainties of the non-dimensional parameters for each of the measured physical properties are summarized in Table 5.

Table 5. Uncertainties for the values of the relevant variables.

Variable	Uncertainty (%)
Velocity of fluid (U)	5
Mean temperature (T)	0.25
Diameter of the nozzle (D_h)	0.1
Voltage (V)	0.1
Current (I)	0.72
Dynamic viscosity of the air (μ) (from tables)	0.048
Thermal conductivity of the air (k) (from tables)	0.34
Density of the air (ρ) (from tables)	0.008

3. Results

In this study, the HT characteristics of a rectangular finned heat sink, previously optimized using the Taguchi $L_{27}(3^{11})$ experimental method, were examined under impinging jet conditions [21,35]. The optimized heat sink was analyzed for the effects of different heat sink angles, nozzle diameters, h/d ratios, and velocity values under constant heat flux. The experiments were conducted with three nozzle diameters (d = 25, 32, and 40 mm), three heat sink angles (α = 10°, 20°, and 30°), three h/d ratios (h/d = 6, 7, and 8), and five velocity values (V = 5, 6, 7, 8, and 9 m/s).

The Nu rose concurrently with Re in all instances. However, the rate of growth fluctuated based on the nozzle diameter and the velocity of the jet air. Increased nozzle widths resulted in higher Nus. The optimal thermal performance was attained with the biggest nozzle diameter (D = 40 mm), followed by the 32 mm diameter, but the smallest diameter (25 mm) demonstrated the least effective thermal performance. The Nusselt number grew as the height-to-diameter ratio fell, exhibiting a generally linear relationship. Furthermore, while the Nus for various heat sink angles were similar, a reduction in the heat sink angle led to an elevation in the Nu.

3.1. Variation in Nusselt Number with Re

3.1.1. Comparison of Experimental Results for Inclined Heat Sink (α = 10°)

For the rectangular, finned heat sink inclined at 10°, the Nu increased with increasing Re. An increase in the nozzle diameter and jet air velocity also contributed to higher Nus. Conversely, the Nu increased with a decreasing h/d ratio, with the relationship being largely linear. The variations in Nus with Res for dimensionless distances (h/d = 6, 7, 8) are presented in Figures 3–5.

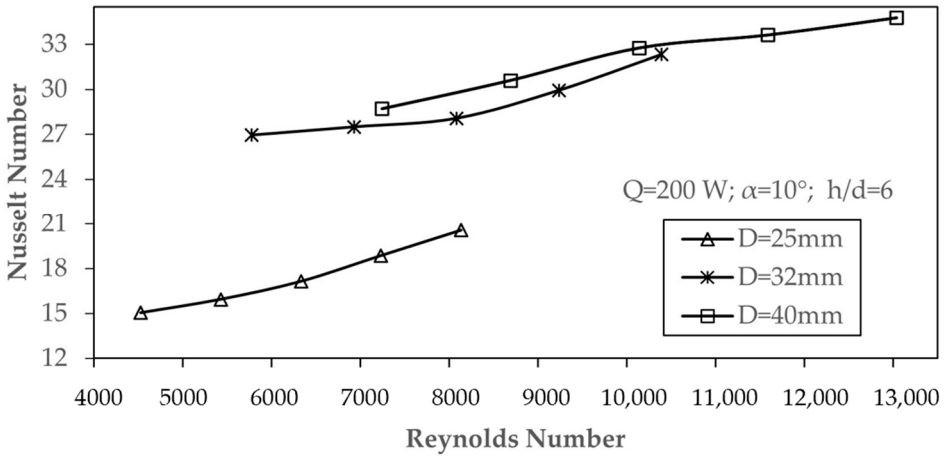

Figure 3. Comparison of experimental results for inclined heat sink (α = 10°) at constant heat flux (200 W) and h/d = 6.

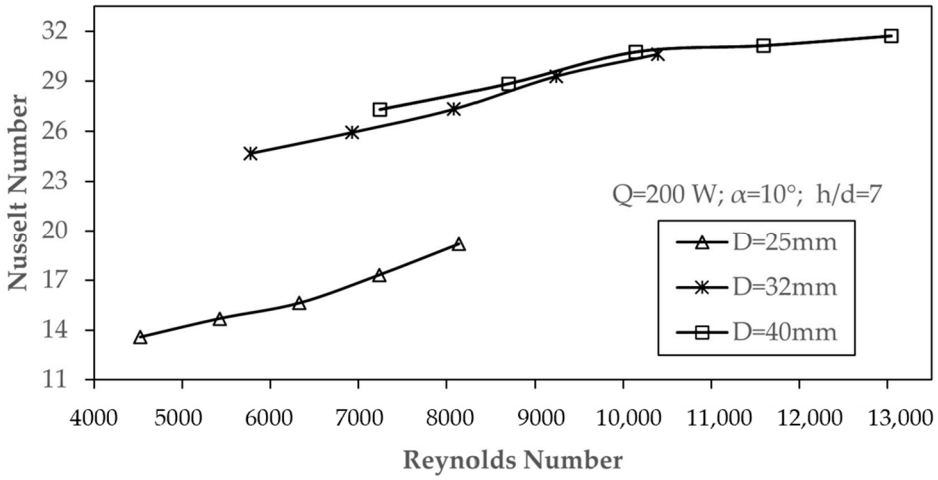

Figure 4. Comparison of experimental results for inclined heat sink (α = 10°) at constant heat flux (200 W) and h/d = 7.

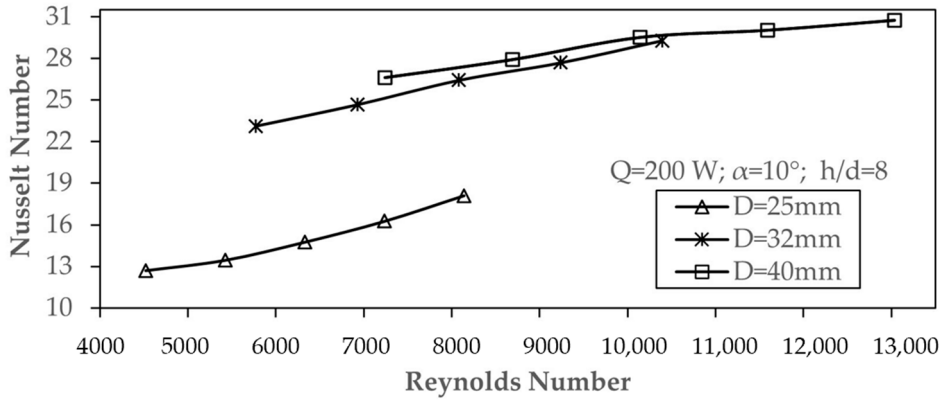

Figure 5. Comparison of experimental results for inclined heat sink (α = 10°) at constant heat flux (200 W) and h/d = 8.

The experimental results of the Nu-Re variation for five different velocity values, considering a rectangular, finned, 10° inclined heat receiver at a constant heat flux of 200 W, under different nozzle-to-heat sink distances (normalized by nozzle diameter) and nozzle diameters, are presented in Figure 3. Considering the experimental results, it was observed that the Nu increased with the rising Re and nozzle diameter. Conversely, it was determined that the Nu increased as the dimensionless h/d distance decreased, and this relationship was predominantly linear. While the Nu was similarly affected across all jet velocity levels, it exhibited a more significant impact at higher speeds, particularly around 7 m/s, compared to lower velocities. For all nozzle diameters and nozzle-to-heat sink distances normalized by the nozzle diameter, the Nu reached its maximum value at the highest flow speed (9.0 m/s). At a constant heat flux, the highest Nu for the rectangular, finned, 10° inclined heat receiver was calculated for a nozzle diameter of D = 40 mm, at a distance of h/d = 6, and a flow velocity of 9 m/s.

For a constant heat flux, at a nozzle diameter of D = 25 mm and a distance of h/d = 6, the Nu of the rectangular finned, 10° inclined heat sink showed an increase in the range of 6–10% between consecutive velocity increments. Furthermore, under the same conditions, an increase of 36.8% for the Nu was found between the minimum (4.0 m/s) and maximum (9.0 m/s) velocities. For a nozzle diameter of D = 32 mm at h/d = 6, the increase in the Nu was between 2% and 8% for consecutive velocity increments, with a total increase of 19.8% between the minimum and maximum velocities. Similarly, for a nozzle diameter of

D = 40 mm at h/d = 6, the Nu showed an increase of 2.7–7% between consecutive velocity increments and a total increase of 21.1% between the minimum and maximum velocities. According to the experimental results for the constant heat flux (200 W) and inclined heat sink (α = 10°) at h/d = 6, it was observed that the heat transfer was enhanced as the fluid velocity and nozzle diameter increased.

For h/d = 7, with a nozzle diameter of D = 25 mm, the Nu exhibited a rise of 6.4–10.9% between consecutive velocities and a total increase of 41.6% between the minimum and maximum velocities. For D = 32 mm, the corresponding increases were 4.5–7.2% between consecutive velocities and 24.1% between the minimum and maximum velocities. For D = 40 mm, the increments ranged from 1.2% to 6.6% for consecutive velocities, with a total increase of 16.1% between the minimum and maximum velocities. The experimental results for a constant heat flux of 200 W and an inclined heat sink at an angle of 10° with a height-to-diameter ratio of seven indicated that the heat transfer enhanced with the increasing fluid velocity and nozzle diameter.

The experimental results for a constant heat flux of 200 W and an inclined heat sink at an angle of 10° with a height-to-diameter ratio of eight indicated that heat transfer enhanced with the increasing fluid velocity and nozzle diameter. For h/d = 8, with a nozzle diameter of D = 25 mm, the Nu showed an increase of 5.9–11.4% between consecutive velocity increments and a total increase of 42.6% between the minimum and maximum velocities. For D = 32 mm, the increases ranged from 4.7% to 7.2% between consecutive velocities and 26.6% between the minimum and maximum velocities. Finally, for D = 40 mm, the increments were between 1.8% and 5.8% for consecutive velocities, with a total increase of 15.7% between the minimum and maximum velocities.

The Nus corresponding to the maximum and minimum flow velocities for a rectangular finned heat sink inclined at 10° were compared for the same nozzle diameter across varying ratios of the h/d to nozzle diameter. At a dimensionless distance of h/d = 6 and h/d = 7 and a nozzle diameter of 25 mm, a 9.8% reduction in the Nu was observed between minimum velocities (4.0 m/s), and a 6.7% reduction was observed between maximum velocities (9.0 m/s). Similarly, for a nozzle diameter of 32 mm, a 6.3% reduction in the Nu was observed between minimum velocities and a 5.3% reduction was observed between maximum velocities. For a nozzle diameter of 40 mm, the Nu decreased by 4.8% at minimum velocities and by 8.7% at maximum velocities. Between h/d = 7 and h/d = 8, with a nozzle diameter of 25 mm, the Nu decreased by 6.3% at minimum velocities and by 5.7% at maximum velocities. For a nozzle diameter of 32 mm, a 6.2% reduction was noted at minimum velocities, and a 4.3% reduction was observed at maximum velocities. For a nozzle diameter of 40 mm, the reductions were 2.6% at minimum velocities and 3% at maximum velocities. When the dimensionless distances h/d = 6 and h/d = 8 were compared for a nozzle diameter of 25 mm, the Nu decreased by 15.6% at minimum velocities and by 12% at maximum velocities. For a nozzle diameter of 32 mm, the reductions were 14.2% at minimum velocities and 9.4% at maximum velocities. For a nozzle diameter of 40 mm, the reductions were 7.3% at minimum velocities and 11.5% at maximum velocities.

3.1.2. Comparison of Experimental Results for Inclined Heat Sink (α = 20°)

The Nu for a rectangular finned heat sink with a 20° inclination increased with the increase in Res. Increases in the nozzle diameter and jet air velocity also led to higher Nus. Conversely, the Nu increased with a decreasing dimensionless h/d distance, and the relationship was predominantly linear. The results illustrating the variation in Nus with Res for dimensionless distances (h/d = 6, 7, 8) are presented in Figures 6–8.

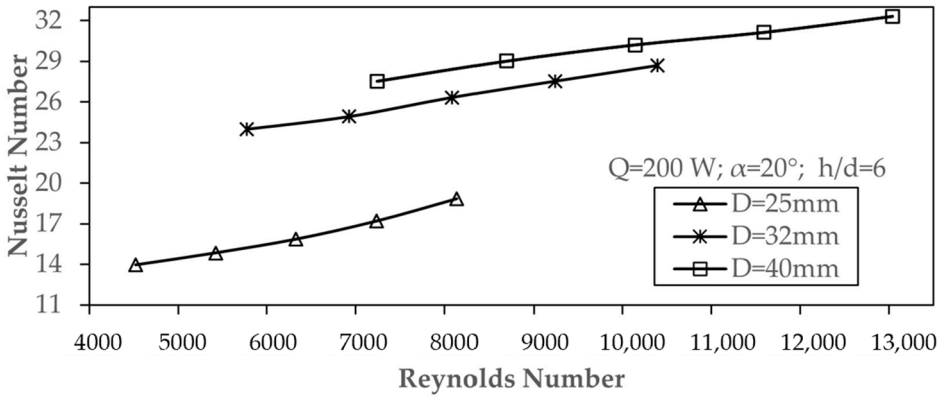

Figure 6. Comparison of experimental results for inclined heat sink (α = 20°) at constant heat flux (200 W) and h/d = 6.

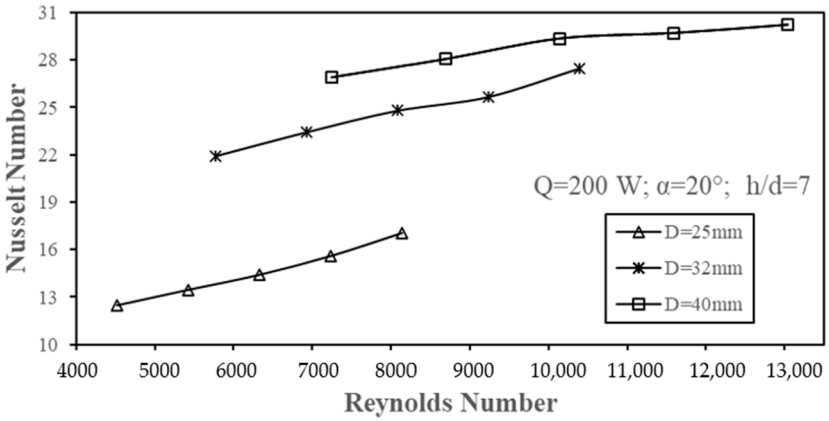

Figure 7. Comparison of experimental results for inclined heat sink (α = 20°) at constant heat flux (200 W) and h/d = 7.

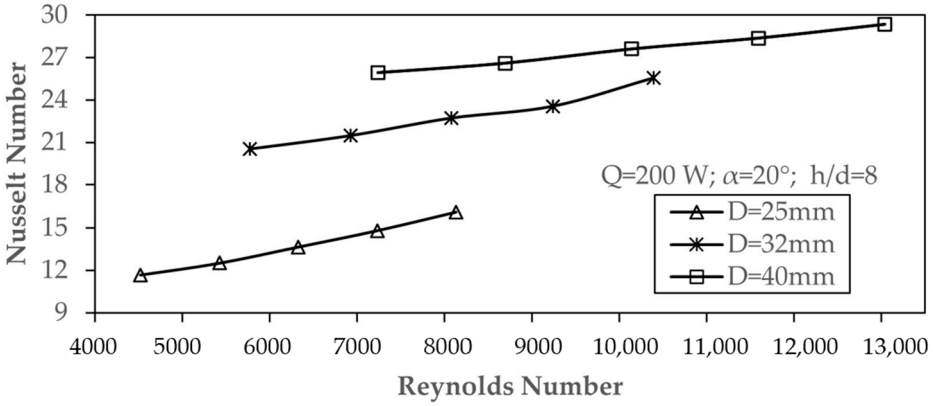

Figure 8. Comparison of experimental results for inclined heat sink (α = 20°) at constant heat flux (200 W) and h/d = 8.

Figures 6–8 present the experimental results of Nu-Re variations for a rectangular finned heat sink inclined at 20° under a constant heat flux of 200 W. The results cover varying ratios of the h/d to nozzle diameter and different nozzle diameters for five flow velocity values. Based on the experimental results, it was determined that the Nu increases with higher Res and larger nozzle diameters. However, the Nu also increases as the dimensionless h/d distance decreases, with a predominantly linear relationship.

While the Nu is affected almost uniformly across all jet velocity levels, it is more significantly influenced at moderate speeds (approximately 7 m/s) than at lower speeds. For

all nozzle diameters and nozzle-to-heat sink distance ratios, the Nu reaches its maximum value at the highest flow velocity (9.0 m/s). The maximum Nu for the rectangular finned heat sink with a 20° inclination under constant heat flux conditions was calculated at a nozzle diameter of 40 mm, a dimensionless distance of h/d = 6, and a flow velocity of 9 m/s.

For the rectangular, finned heat sink with a nozzle diameter of 25 mm and a dimensionless distance of h/d = 6, an increase in flow velocity resulted in a 6.4% to 9.6% increase in the Nu. Additionally, a 35% increase in the Nu was found between minimum (4.0 m/s) and maximum (9.0 m/s) velocities under the same conditions. For a nozzle diameter of 32 mm, increases in flow velocity resulted in a 3.9% to 5.7% rise in the Nu, with a 19.7% increase observed between the minimum and maximum velocities under the same conditions. For a nozzle diameter of 40 mm, the Nu increased by 3% to 5.4% with rising flow velocity and a 17.4% increase was observed between the minimum and maximum velocities under the same conditions. According to the experimental results for the constant heat flux (200 W) and inclined heat sink ($\alpha = 20°$) at h/d = 6, it was observed that the heat transfer became enhanced as the fluid velocity and nozzle diameter increased.

Under constant heat flux conditions, for a rectangular, finned heat sink inclined at 20° with a nozzle diameter of 25 mm and a dimensionless distance of h/d = 7, an increase in Nu values ranging from 7.1% to 9.4% was observed due to successive increments in velocity. Additionally, for the rectangular, finned heat sink under the same conditions, a 36.8% increase in the Nu was recorded between the minimum (4.0 m/s) and maximum (9.0 m/s) velocities. Similarly, with a nozzle diameter of 32 mm and a dimensionless distance of h/d = 7, the Nu increased by 3.5% to 7% as velocity increased incrementally. Under the same conditions, a 25.3% increase in the Nu was found between the minimum (4.0 m/s) and maximum (9.0 m/s) velocities. For a nozzle diameter of 40 mm and h/d = 7, the increase in Nu due to successive velocity increments ranged between 1.2% and 4.6%. Moreover, a 12.5% increase was observed in the Nu between the minimum and maximum velocities under the same conditions. The experimental results for a constant heat flow of 200 W and an inclined heat sink at a 20° angle, with a height-to-diameter ratio of seven, demonstrated that heat transfer is enhanced by increasing fluid velocity and nozzle diameter.

For a rectangular finned heat sink inclined at 20° with a constant heat flux and a nozzle diameter of 25 mm at h/d = 8, the Nu increased by 7.1% to 9.1% due to successive velocity increments. Additionally, a 37.8% increase in the Nu was found between the minimum (4.0 m/s) and maximum (9.0 m/s) velocities. With a nozzle diameter of 32 mm and h/d = 8, the Nu increased by 3.7% to 8.5% due to incremental velocity increases, while a 24.5% increase was observed between the minimum and maximum velocities. For a nozzle diameter of 40 mm at h/d = 8, the Nu increased by 2.6% to 3.8% due to successive velocity increments, and a 13.2% increase was recorded between the minimum and maximum velocities. The experimental results for constant heat flux of 200 W and an inclined heat sink at an angle of 20° with a height-to-diameter ratio of eight indicated that heat transfer enhanced with an increasing fluid velocity and nozzle diameter.

At a heat flux of 200 W, the Nus for varying nozzle-to-heat-sink dimensionless distances and the same nozzle diameter were compared for minimum and maximum flow velocities. Between the dimensionless distances of h/d = 6 and h/d = 7, for a nozzle diameter of 25 mm, a 10.5% decrease in the Nu was found for the minimum velocity (4.0 m/s), and a 9.4% decrease was found for the maximum velocity (9.0 m/s). For a nozzle diameter of 32 mm, decreases of 8.6% and 4.3% were found for minimum and maximum velocities, respectively, under the same dimensionless distance comparison. For a nozzle diameter of 40 mm, the Nu decreased by 2.4% for the minimum velocity and by 6.5% for the maximum velocity between h/d = 6 and h/d = 7.

For the dimensionless distances of h/d = 7 and h/d = 8, with a nozzle diameter of 25 mm, the Nu decreased by 6.4% and 5.7% for the minimum and maximum velocities, respectively. For a nozzle diameter of 32 mm, decreases of 6.4% and 7% were observed for the minimum and maximum velocities, respectively. With a nozzle diameter of 40 mm, the Nu decreased by 3.5% for the minimum velocity and by 2.9% for the maximum velocity.

Between h/d = 6 and h/d = 8, for a nozzle diameter of 25 mm, the Nu decreased by 16.3% for the minimum velocity and by 14.5% for the maximum velocity. For a nozzle diameter of 32 mm, decreases of 14.5% and 11% were observed for the minimum and maximum velocities, respectively. For a nozzle diameter of 40 mm, the Nu decreased by 5.9% for the minimum velocity and by 9.2% for the maximum velocity.

3.1.3. Comparison of Experimental Results for Inclined Heat Sink (α = 30°)

The Nu for the rectangular finned heat sink inclined at 30° increased with the Re. An increase in nozzle diameter and jet air velocity led to a rise in the Nu. Conversely, the Nu increased with a decreasing dimensionless h/d distance, and the relationship was predominantly linear. The variation in the Nu with the Re for different dimensionless distances (h/d = 6, 7, and 8) is presented in Figures 9–11.

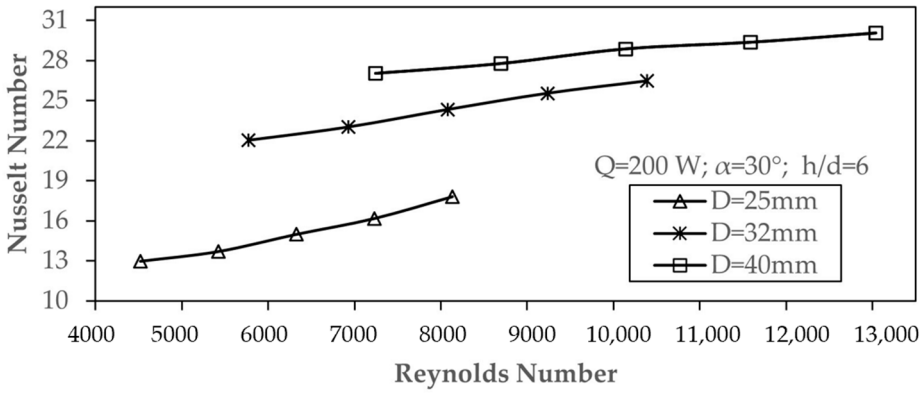

Figure 9. Comparison of experimental results for inclined heat sink (α = 30°) at constant heat flux (200 W) and h/d = 6.

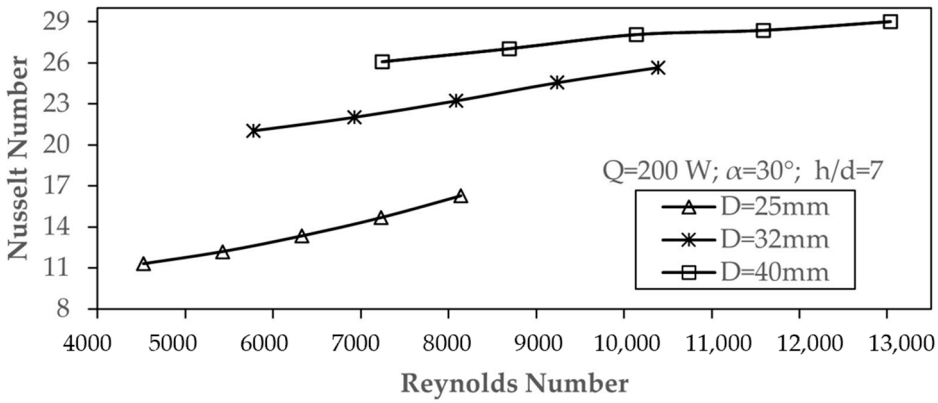

Figure 10. Comparison of experimental results for inclined heat sink (α = 30°) at constant heat flux (200 W) and h/d = 7.

The experimental results of Nu-Re variations for five different velocity values under the influence of different nozzle-to-receiver, distance-to-nozzle diameter ratios, and nozzle diameters for a rectangular-finned, 30° inclined heat receiver with a constant heat flux of 200 W are presented in Figures 9–11. The experimental findings indicate that the Nu increases with higher Res and larger nozzle diameters. Conversely, the Nu also increased

with the decreasing dimensionless h/d distance, and the relationship was predominantly linear. The Nu was nearly uniformly affected across all jet velocities but showed a more significant impact at approximately 7 m/s compared to lower velocities. For all nozzle diameters and nozzle-to-receiver, distance-to-diameter ratios, the Nu reached its maximum value at the highest flow velocity of 9.0 m/s. At constant heat flux, the highest Nu for the rectangular-finned, 30° inclined heat receiver was calculated for a nozzle diameter of 40 mm, an h/d distance of six, and a flow velocity of 9 m/s.

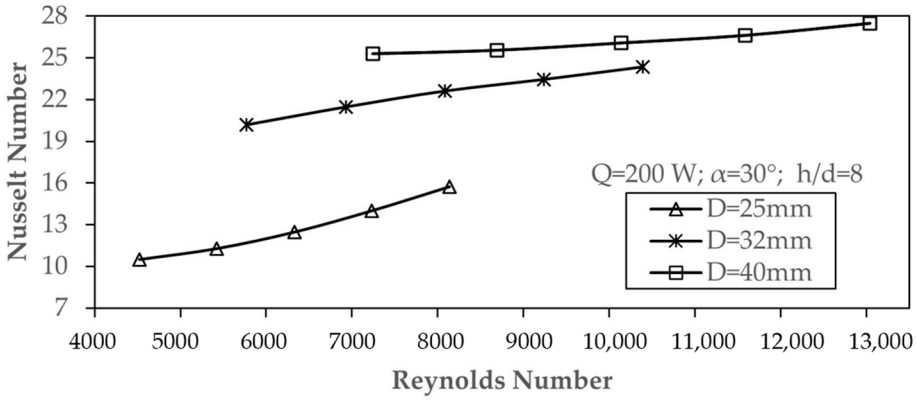

Figure 11. Comparison of experimental results for inclined heat sink (α = 30°) at constant heat flux (200 W) and h/d = 8.

For a rectangular-finned, 30° inclined heat receiver with constant heat flux, a nozzle diameter of 25 mm, and an h/d distance of six, the Nu increased between 5.6% and 10.2% with successive velocity increments. Additionally, under the same conditions, a 37.4% increase in the Nu was found between the minimum (4.0 m/s) and maximum (9.0 m/s) velocities. For a nozzle diameter of 32 mm and an h/d distance of six, the Nu increased between 3.6% and 5.7% with successive velocity increments, while a 20.2% increase was observed between the minimum and maximum velocities. For a nozzle diameter of 40 mm and an h/d distance of six, the Nu increased between 1.7% and 4% with successive velocity increments, and an 11.2% increase was observed between the minimum and maximum velocities. According to the experimental results for the constant heat flux (200 W) and inclined heat sink (α = 30°) at h/d = 6, it was observed that the heat transfer enhanced as the fluid velocity and nozzle diameter increased.

For a rectangular-finned, 30° inclined heat receiver with constant heat flux, a nozzle diameter of 25 mm, and an h/d distance of seven, the Nu increased between 7.9% and 10.8% with successive velocity increments. Under the same conditions, a 44% increase in the Nu was found between the minimum (4.0 m/s) and maximum (9.0 m/s) velocities. For a nozzle diameter of 32 mm and an h/d distance of seven, the Nu increased between 4.5% and 5.8% with successive velocity increments, and a 22.1% increase was observed between the minimum and maximum velocities. For a nozzle diameter of 40 mm and an h/d distance of seven, the Nu increased between 1.1% and 3.9% with successive velocity increments, while an 11.4% increase was observed between the minimum and maximum velocities. The experimental results for a constant heat flux of 200 W and an inclined heat sink at an angle of 30° with a height-to-diameter ratio of seven enhanced that heat transfer with increasing fluid velocity and nozzle diameter.

Under constant heat flux conditions, for a rectangular, finned heat sink with a 30° inclination and a nozzle diameter of 25 mm at an h/d ratio of eight, an increase in the Nu ranging from 7.5% to 12.4% was observed with successive increments in velocity values. Additionally, for the same heat sink under identical conditions, the Nu exhibited a 49.9% increase between the minimum velocity (4.0 m/s) and the maximum velocity (9.0 m/s).

For a nozzle diameter of 32 mm under constant heat flux conditions and the same h/d ratio of eight, the Nu increased by 3.7% to 6.3% with successive increments in velocity. Furthermore, under identical conditions, a 20.5% increase in the Nu was found between the minimum (4.0 m/s) and maximum (9.0 m/s) velocities. For a nozzle diameter of 40 mm, under constant heat flux conditions and an h/d ratio of eight, the Nu increased by 1.0% to 3.2% with successive velocity increments. Additionally, for the same heat sink and conditions, an 8.6% increase in the Nu was noted between the minimum (4.0 m/s) and maximum (9.0 m/s) velocities. The experimental results for a constant heat flux of 200 W and an inclined heat sink at an angle of 30° with a height-to-diameter ratio of eight indicated that heat transfer enhanced with the increasing fluid velocity and nozzle diameter.

At a heat flux of 200 W, the Nus corresponding to maximum and minimum flow velocities were compared for the same heat sink with varying nozzle-to-heat sink distances normalized by the nozzle diameter. Between the h/d ratios of six and seven for a 25 mm nozzle diameter, a 12.8% decrease in the Nu was observed at minimum velocity (4.0 m/s), while a decrease of 8.6% was recorded at maximum velocity (9.0 m/s). For a 32 mm nozzle diameter between the same h/d ratios, the Nu decreased by 4.5% at a minimum velocity and by 3.0% at a maximum velocity. Similarly, for a 40 mm nozzle diameter, the Nu exhibited a 3.6% decrease at minimum velocity and a 3.4% decrease at maximum velocity. Between the h/d ratios of seven and eight for a 25 mm nozzle diameter, the Nu showed a decrease of 7.2% at minimum velocity and 3.4% at maximum velocity. For a 32 mm nozzle diameter, the decrease in the Nu was 4.0% at minimum velocity and 5.3% at maximum velocity. For a 40 mm nozzle diameter, decreases of 3.0% and 5.4% were observed at minimum and maximum velocities, respectively. Between h/d ratios of six and eight, for a 25 mm nozzle diameter, the Nu decreased by 19.1% at minimum velocity and by 11.7% at maximum velocity. For a 32 mm nozzle diameter, decreases of 8.3% and 8.1% were observed at minimum and maximum velocities, respectively. For a 40 mm nozzle diameter, the Nu showed reductions of 6.4% at minimum velocity and 8.6% at maximum velocity.

4. Conclusions

Thermal management at a high heat flux is crucial for electronic devices, and jet impingement cooling is a promising solution. Today, the efficiency of the heat sink is one of the most important parameters when designing a heat sink. High-efficiency heat sinks enhance heat transfer. This experimental study was carried out to investigate HT phenomena and the associated flow characteristics on a heat sink surface consisting of rectangular fins with a converging–diverging geometry, cooled by the air as the coolant, using multi-impingement jets on inclined surfaces. Considering the importance of analyzing the effect of the heat sink angle, nozzle diameter, dimensionless distance, and flow rate variables on the heat transfer performance of jet impingement systems, this study aims to provide scientifically proven answers to the industry. The results obtained from the experimental analysis are summarized as follows.

- ✓ The experimental results revealed that the Nu increased with a higher Re.
- ✓ It was calculated that the Nu increased with larger nozzle diameters.
- ✓ However, it was also concluded that the Nu decreased as the dimensionless h/d distance increased, and this relationship was found to be mostly linear.
- ✓ While the Nu was almost equally affected across all jet velocity levels, it was more significantly influenced at lower velocities, specifically at around 7 m/s.
- ✓ Under all the inclined heat sink surface conditions examined, the Nu reached its maximum value at the flow velocity of 9.0 m/s, which corresponded to the points where the nozzle diameters and the dimensionless nozzle-to-heat sink distance ratios were at their optimum.

- ✓ When comparing the angle values for the same flow velocity, nozzle diameter, and dimensionless h/d distance experimental conditions, the Nus were found to be very similar. It was determined that the heat sink angle values examined compared to other parameters had less effect on heat transfer.
- ✓ Under constant heat flux and across all examined angle values, the highest Nu for the inclined heat sink with rectangular fins was calculated at a 10° heat sink inclination, with a nozzle diameter (D) of 40 mm, a dimensionless distance (h/d) of six, and a flow velocity of 9 m/s.
- ✓ Conversely, the lowest Nu was observed at a 30° heat sink inclination, with a nozzle diameter (D) of 25 mm, a dimensionless distance (h/d) of eight, and a flow velocity of 5 m/s.

After examining the parameters affecting impingement jet cooling, the analyses performed according to the single variable method can provide new perspectives for the optimization of jet impingement cooling systems and offer potential improvements for thermal performance and efficiency. The next step is to carry out numerical and experimental research on the impact of the cooling effect of impinging jets using different fluids, a larger number of parameters, and under a wider parameter range, building a relevant test platform and providing more guidance and data for the application of this technology.

Author Contributions: Supervision, A.K.; investigation, D.Y. All authors have read and agreed to the published version of the manuscript.

Funding: This research was supported as a project (BAP-FYL 2021-9534) of the Research Fund of Van Yuzuncu Yil University.

Institutional Review Board Statement: Not applicable.

Informed Consent Statement: Not applicable.

Data Availability Statement: The data presented in this study are available on request from the corresponding author.

Conflicts of Interest: The authors declare no conflicts of interest.

Abbreviations

The following abbreviations are used in this manuscript:

A	Area (m^2)
b	Width of fin (m)
c_p	Pressure coefficient (J kg^{-1} K^{-1})
D	Nozzle diameter (m)
h	Convection coefficient (W m^{-2} K)
H	Height of fin (m)
h/D	Dimensionless distance between nozzle–target surface (dimensionless)
I	Current (A)
k	Thermal conductivity of air (W m^{-1} $K^{-1)}$
L	Length of the base plate (m)
N	Number of fins
Nu	Nusselt number (hD/k) (dimensionless)
R	Resistance (Ω)
Re	Reynolds number (ρVD/μ) (dimensionless)
T	Temperature (K)
t	Thicknesses of fin (m)
U	Velocity (m s^{-1})
V	Potential (V)
W	Width of the base plate (m)
μ	Dynamic viscosity (kg m^{-1} s^{-1})

ρ	Density (kg m^{-3})
	Subscripts
ave	Average
cond	Conduction
conv	Convection
h	Hydraulic
rad	Radiation
s	Surface
tot	Total

References

1. Karabey, A.; Al-Ani, R.A.A. Numerical determination of cooling performance on heat sink using impingement jet. *Duzce Univ. J. Sci. Technol.* **2023**, *11*, 977–989. [CrossRef]
2. Karabey, A.; Bozdogan, D. Experimental Comparison of Heat and Flow Characteristics of Rectangular Finned Heat Sink and Flat Plate Using Single Nozzle Impingement Air Jet. In Proceedings of the CONV-22: International Symposium on Convective Heat and Mass Transfer, Izmir, Turkey, 5–10 June 2022; pp. 589–596.
3. Culun, P.; Celik, N.; Pihtili, K. Effects of design parameters on a multi jet impinging heat transfer. *Alex. Eng. J.* **2018**, *57*, 4255–4266. [CrossRef]
4. Baghel, K.; Sridharan, A.; Murallidharan, J.S. Experimental and numerical study of inclined free surface liquid jet impingement. *Int. J. Therm. Sci.* **2020**, *154*, 106389. [CrossRef]
5. Manay, E.; Şahin, B.; Dilek, E.F. Mikrokanallarda nanoakışkanların kullanımı. *TMMOB MMO Mühendis Makine Derg.* **2012**, *53*, 38–42.
6. Singhal, V.; Garimella, S.V. Induction electro hydrodynamics micropump for high heat flux cooling. *Sens. Actuators A Phys.* **2007**, *134*, 650–659. [CrossRef]
7. Karabey, A.; Yakut, K. Analyzing the heat and flow characteristics in spray cooling by using an optimized rectangular finned heat sink. *Heat Transf. Res.* **2024**, *55*, 19–34. [CrossRef]
8. Yakut, R. Response surface methodology-based multi-nozzle optimization for electrospray cooling. *Appl. Therm. Eng.* **2024**, *236*, 121914. [CrossRef]
9. Kabakus, A.; Yakut, K. Optimization of finned heat sinks with electrospray cooling: Full factorial method. *Heat Transf. Res.* **2024**, *55*, 47–64. [CrossRef]
10. Yesildal, F.; Yakut, K. Optimization of the spray cooling parameters for a heat sink by The Taguchi Method. *At. Sprays* **2017**, *27*, 1063–1075. [CrossRef]
11. Wang, C.Y.; Li, Z.; Xu, P.; Hou, Y.Q.; Tan, D.P.; Li, L. Collision modelling approach and transient response mechanism of ring-ribbed cylindric shells for underwater vehicles. *Appl. Math. Model.* **2025**, *141*, 115923. [CrossRef]
12. Li, L.; Tan, Y.F.; Xu, W.X.; Ni, Y.S.; Yang, J.G.; Tan, D.P. Fluid-induced transport dynamics and vibration patterns of multiphase vortex in the critical transition states. *Int. J. Mech. Sci.* **2023**, *252*, 108376. [CrossRef]
13. Tosun, C. Determination of Heat and Flow Characteristics of Mini Heat Sinks with Cascade Impingement Jet. Ph.D. Thesis, Atatürk University, Erzurum, Turkey, 2024.
14. Karabey, A. Determination of Heat and Flow Characteristics of Impingement Jet for Heat Sink. Master's Thesis, Atatürk Uni-versity, Erzurum, Turkey, 2010.
15. Maghrabie, H.M. Heat transfer intensification of jet impingement using exciting jets—A comprehensive review. *Renew. Sustain. Energy Rev.* **2021**, *139*, 110684. [CrossRef]
16. Yildizeli, A.; Cadirci, S. Multi-objective optimization of multiple impinging jet system through genetic algorithm. *Int. J. Heat Mass Transf.* **2020**, *158*, 119978. [CrossRef]
17. Bhaumik, M.; Dhanawade, K.; Sur, A. A numerical model analysis on perforated aerofoil shaped pin fin arrays in heat dissipation enhancement, pressure drop and optimization. *Mater. Today Proc.* **2023**, *92*, 1319–1333. [CrossRef]
18. Kim, T.; Jung, E.Y.; Bang, M.; Lee, C.; Moon, H.K.; Cho, H.H. Heat transfer measurements for array jet impingement with castellated wall. *J. Turbomach.* **2022**, *144*, 031009. [CrossRef]
19. Yang, X.; Wu, H.; Feng, Z. Jet impingement heat transfer characteristics with variable extended jet holes under strong crossflow conditions. *Aerospace* **2022**, *9*, 44. [CrossRef]
20. Rabbani, G.; Singh, D. Large Eddy simulation of turbulent slot jet impingement on heated flat plate. In *Recent Advances in Mechanical Engineering, Lectures Notes in Mechanical Engineering*; Springer: Singapore, 2021; pp. 795–806.
21. Karabey, A.; Arvasi, S. Optimization of the design parameters using the Taguchi Method in inclined impingement multijet heat transfer with rectangular finned heat sink. *Heat Transf. Res.* **2023**, *54*, 37–51. [CrossRef]

22. Karabey, A.; Al-Ani, R.A.A.; Bozdogan, D. Experimental and numerical investigation of flow and heat transfer characteristics using impinging jet on optimized rectangular finned heat sinks. *Heat Transf. Res.* **2022**, *53*, 61–77. [CrossRef]
23. Guresci, K.; Yesildal, F.; Karabey, A.; Yakut, R.; Yakut, K. Numerical analysis with experimental comparison in duct flow using optimized heat sinks. *J. Radiat. Res. Appl. Sci.* **2018**, *11*, 116–123.
24. Jung, E.Y.; Park, C.U.; Lee, D.H.; Kim, K.M.; Woo, T.K.; Cho, H.H. Heat transfer characteristics of an angled array impinging jet on a concave duct. In Proceedings of the ASME Turbo Expo 2012: Turbine Technical Conference and Exposition, Copenhagen, Denmark, 11–15 June 2012; American Society of Mechanical Engineers (ASME): New York, NY, USA, 2012; Volume 4, pp. 601–607.
25. Jung, E.Y.; Park, C.U.; Lee, D.H.; Kim, K.M.; Cho, H.H. Effect of the injection angle on local heat transfer in a showerhead cooling with array impingement jets. *Int. J. Therm. Sci.* **2018**, *124*, 344–355. [CrossRef]
26. Heo, M.W.; Lee, K.D.; Kim, K.Y. Parametric study and optimization of staggered inclined impinging jets on a concave surface for heat transfer augmentation. *Numer. Heat Transf. Part A Appl.* **2012**, *61*, 442–462. [CrossRef]
27. Ravanji, A.; Zargarabadi, M.R. Effects of pin-fin shape on cooling performance of a circular jet impinging on a flat surface. *Int. J. Therm. Sci.* **2021**, *161*, 106684. [CrossRef]
28. Lu, X.; Li, W.; Li, X.; Ren, J.; Jiang, H.; Ligrani, P. Flow and heat transfer characteristics of micro pin-fins under jet impingement arrays. *Int. J. Heat Mass Transf.* **2019**, *143*, 118416. [CrossRef]
29. Smith, A.H.; Bhavnani, S.H.; Knight, R.W. Promoting fountain behaviors with cone surface structures under impinging jets. *Appl. Therm. Eng.* **2023**, *232*, 120888. [CrossRef]
30. Nourin, F.N.; Amano, R.S. Heat transfer augmentation with multiple jet impingement cooling on dimpled surface for gas turbine blades. *ASME J. Energy Resour. Technol.* **2023**, *145*, 022101. [CrossRef]
31. Nada, S.A. Buoyancy and cross flow effects on heat transfer of multiple impinging slot air jets cooling a flat plate at different orientations. *Heat Mass Transfer.* **2009**, *45*, 1083–1097. [CrossRef]
32. Barbosa, F.V.; Teixeira, S.F.; Teixeira, J.C. Heat transfer and fluid dynamics of a single jet impingement-An experimental and numerical approach. *Int. J. Therm. Science.* **2024**, *200*, 108993. [CrossRef]
33. Cengel, Y.A.; Cimbala, J.M. *Fluid Mechanics. Fundamentals and Applications*, 3rd ed.; McGraw-Hill: New York, NY, USA, 2014.
34. Kline, S.J.; McClintock, F.A. Describing uncertainties in single-sample experiments. *ASME Mech. Eng.* **1953**, *75*, 3–8.
35. Arvasi, S. Optimization of Heat Sink Design Parameters in Multi-Impinging Jet Heat Transfer by Taguchi Method. Master's Thesis, Van Yüzüncü Yıl University, Van, Turkey, 2022.

Disclaimer/Publisher's Note: The statements, opinions and data contained in all publications are solely those of the individual author(s) and contributor(s) and not of MDPI and/or the editor(s). MDPI and/or the editor(s) disclaim responsibility for any injury to people or property resulting from any ideas, methods, instructions or products referred to in the content.